Supporting Information for "A synoptic view of mantle plume shapes enabled by virtual reality"

Qianyi Lu, Maxwell L. Rudolph[1]

[1]Department of Earth and Planetary Sciences, University of California, Davis, Davis, CA, USA

Contents of this file

1. Text S1 to S3

2. Figures S1 to S7

3. Tables S1

Introduction In Text S1, we describe how we construct the reference $d\ln V_S/dT$ profile along depth in more details. In Text S2, we evaluate the slowness of our two sets of traced conduits in multiple other global tomographic models and discuss where the mutual consistency and disagreement are. In Text S3, we provides more examples of how to trace conduit of plumes that have multiple possible candidate conduits or the traced conduits do not strictly follow our criteria. We also provide more cross sections of plumes that we traced in this study (Figure S2-6) and a table of the locations, buoyancy flux, and information about whether the traced conduits agree with the modeled conduits of all traced plumes.

Text S1. $d\ln V_S/dT$ **profile**

The $d\ln V_S/dT$ profile (Figure S1) beneath 800 km is calculated in Burnman (Cottaar et

al., 2014; Myhill et al., 2021) assuming the phases at these depths are 82% perovskite [$(Mg_{0.9}Fe_{0.1})SiO_3$] and 18% ferropericlase [$(Mg_{0.8}Fe_{0.2})O$]. The profile above 800 km depth is adapted from Cammarano, Goes, Vacher, and Giardini (2003). Although the mantle composition used in Burnman are not in mass conversation with the mantle composition used in Cammarano et al. (2003), it is a reasonable composition of a pyrolitic lower mantle. We believe that the $d\ln V_S/dT$ profile we calculate is accurate enough for our purpose of use.

Text S2. Slowness of trace plume conduits in other tomographic models.

To evaluate the robustness of our traced conduits, we evaluate the slowness, which is measured as the velocity anomaly, of our two sets of traced conduits traced from SEMUCB-WM1 and GLAD-M25 (V_S) in other global tomographic models, both S-velocity models (GLAD-M25 (V_S)/SEMUCB-WM1 TX2019slab (V_S) and SPiRaL (V_S)) and P-velocity models (GLAD-M25 (V_P), TX2019slab (V_P), SPiRaL (V_P), DETOX-P3, and UU-P07). Here, GLAD-M25 (Lei et al., 2020), TX2019slab (Lu et al., 2019), and SPiRaL (Simmons et al., 2021) are jointly inverted P and S velocity models. DETOX-P3 (Hosseini et al., 2020) and UU-P07 (Amaru, 2007) are purely P-velocity models, where SEMUCB-WM1 is a purely S-velocity model. Among all these tomographic models, only SEMUCB-WM1 and GLAD-M25 are full-waveform models, while the others are body wave travel-time models based on race tracing theory. Only SEMUCB-WM1, GLAD-M25, and DETOX-P3 claim to resolve plumes in the original publications (French & Romanowicz, 2015; Hosseini et al., 2020; Lei et al., 2020), while the others do not make any statement about resolving plumes in their original publications.

March 30, 2024, 11:35pm

The 12 Pacific traced conduits (TCs) from GLAD-M25 are slower than the modeled conduits (MCs) and vertical conduits (VCs) below 660 – 1200 km in all tomographic model except UU-P07 (Figure 5i Figure S2 h-n). The slowness along this set of TCs is generally greater or comparable to the slowness along MCs and TCs. In TX2019slab (V_P and V_S), no MC is slower than TCs at any depth. In SPiRaL (V_P and V_S), the average slowness of TCs is less than the slowness of MCs at about 1500 km (Figure S2 h, k), which is mainly caused by Samoa plume.

The Pacific TCs from SEMUCB-WM1 are slower than MCs and VCS in a more restricted depth range (between $\sim$ 1250 and 2100 km) in GLAD-M25 (V_P), TX2019slab (V_P and V_S), SPiRaL (V_S), and DETOX-P3, but are comparable to MCs and VCs in SPiRaL (V_P) and UU-P07 (Figure 5d Figure S2 a-g). TCs of Easter, Galapagos, and Macdonald plumes are the main contributor of slowness in TX2019slab (V_P and V_S). In SPiRaL (V_P), the average slowness of TCs is indistinguishable to the average slowness of MCs and VCs mostly because TCs of Macdonald, Marquesas, San Felix, and especially Samoa plumes are faster than their MCs and VC in the mid-mantle.

In UU-P07, the average slowness of two sets of TCs, MCs and VCs are comparable to each other and remain close 0% at all depths. This result is not surprising because first, P-velocity is less sensitive to thermal anomaly; second, the resolution of UU-P07 is generally poorer below the ocean (Amaru, 2007), where most of the traced plumes locate. The resolution of TX2019slab (V_P) and DETOX-P3, in which the average slowness of two sets of TCs is greater than the average slowness of MCs and VCs in the mid to lower mantle, has a poor resolution in the upper mantle in the Pacific region but a good resolution in the mid and lower mantle (Lu et al., 2019; Hosseini et al., 2020).

In summary, both sets of traced conduits, especially TCs from GLAD-M25, are more compatible with many other tomographic models than the modeled and vertical conduits in the mid to lower mantle. Our traced condutis should be a better representation of plume shapes than the modeled and vertical conduits.

Text S3. Procedures to trace plume conduits with ambiguity.

Here, we provide some examples of how we decide the traced conduit of a plume over multiple candidate traced conduits of a plume. For example, the traced conduits of Galapagos from SEMUCB-WM1 and GLAD-M25 almost do not have any overlaps but we find that CCs resolved in the two models have overlaps (Figure S4a-b). We traced the most straightforward conduit path below 660 km for Galapagos that connects the CC resolved above 660 km depth in SEMUCB-WM1 (box in Figure S4a) to the CC right beneath this anomaly. If we decide that the upper-mantle CC is connected to the lower-mantle CC resolved in both tomographic models, the conduit traced from SEMUCB-WM1 will have much more overlaps with the conduit traced from GLAD-M25. Similarly for Easter, strongly sheared CC is observed between 660 and $\sim$ 2000 km depth (Figure 9d). The CC resolved in GLAD-M25 below $\sim$ 2000 km favors a conduit sheared towards the northeast, while the CC resolved in SEMUCB-WM1 could be interpreted as either vertical or sheared conduit.

The Tristan plume is thought to form the Tristan-Gough hotspot track and the Parana-Etendeka flood basalts (Richards et al., 1989). The isotopic observations of basalt from the Tristan-Gough hotspot track suggest that they are EM1 and HIMU types, which usually indicates a mantle plume origin. Because of these observations, we include the

conduit of Tristan, although a continuous conduit is only clearly resolved in SEMUCB-WM1 but not in GLAD-M25 (Figure S6). The conduit of Tristan is resolved only below 660 km depth in GLAD-M25. For plume Azores, the CC with large-amplitude negative δV_S between 660 and 1250 km depth in SEMUCB-WM1 makes us decide the conduit to pass through this region while this CSS is not significant in GLAD-M25 (Figure S3c).

References

Amaru, M. L. (2007). Global travel time tomography with 3-d reference models. *Geologica Ultraiectina*, *274*. Retrieved from `https://dspace.library.uu.nl/handle/1874/19338` (Accepted: 2007-02-02T14:51:52Z)

Cammarano, F., Goes, S., Vacher, P., & Giardini, D. (2003). Inferring upper-mantle temperatures from seismic velocities. *Physics of the Earth and Planetary Interiors*, *138*(3), 197–222. doi: 10.1016/S0031-9201(03)00156-0

Cottaar, S., Heister, T., Rose, I., & Unterborn, C. (2014). BurnMan: A lower mantle mineral physics toolkit. *Geochemistry, Geophysics, Geosystems*, *15*(4), 1164–1179. doi: 10.1002/2013GC005122

French, S. W., & Romanowicz, B. (2015). Broad plumes rooted at the base of the Earth's mantle beneath major hotspots. *Nature*, *525*(7567), 95–99. doi: 10.1038/nature14876

Hosseini, K., Sigloch, K., Tsekhmistrenko, M., Zaheri, A., Nissen-Meyer, T., & Igel, H. (2020). Global mantle structure from multifrequency tomography using p, pp and p-diffracted waves. *Geophysical Journal International*, *220*(1), 96–141. doi: 10.1093/gji/ggz394

Lei, W., Ruan, Y., Bozdağ, E., Peter, D., Lefebvre, M., Komatitsch, D., . . . Pugmire, D.

(2020). Global adjoint tomography—model glad-m25. *Geophysical Journal International*, *223*(1), 1–21. doi: 10.1093/gji/ggaa253

Lu, C., Grand, S. P., Lai, H., & Garnero, E. J. (2019). Tx2019slab: A new p and s tomography model incorporating subducting slabs. *Journal of Geophysical Research: Solid Earth*, *124*(11), 11549–11567. doi: 10.1029/2019JB017448

Myhill, R., Cottaar, S., Heister, T., Rose, I., & Unterborn, C. (2021). *BurnMan v1.0.1.* Zenodo. doi: 10.5281/zenodo.5552756

Richards, M. A., Duncan, R. A., & Courtillot, V. E. (1989). Flood Basalts and Hot-Spot Tracks: Plume Heads and Tails. *Science*, *246*(4926), 103–107. doi: 10.1126/science.246.4926.103

Simmons, N. A., Myers, S. C., Morency, C., Chiang, A., & Knapp, D. R. (2021). Spiral: a multiresolution global tomography model of seismic wave speeds and radial anisotropy variations in the crust and mantle. *Geophysical Journal International*, *227*(2), 1366–1391. doi: 10.1093/gji/ggab277
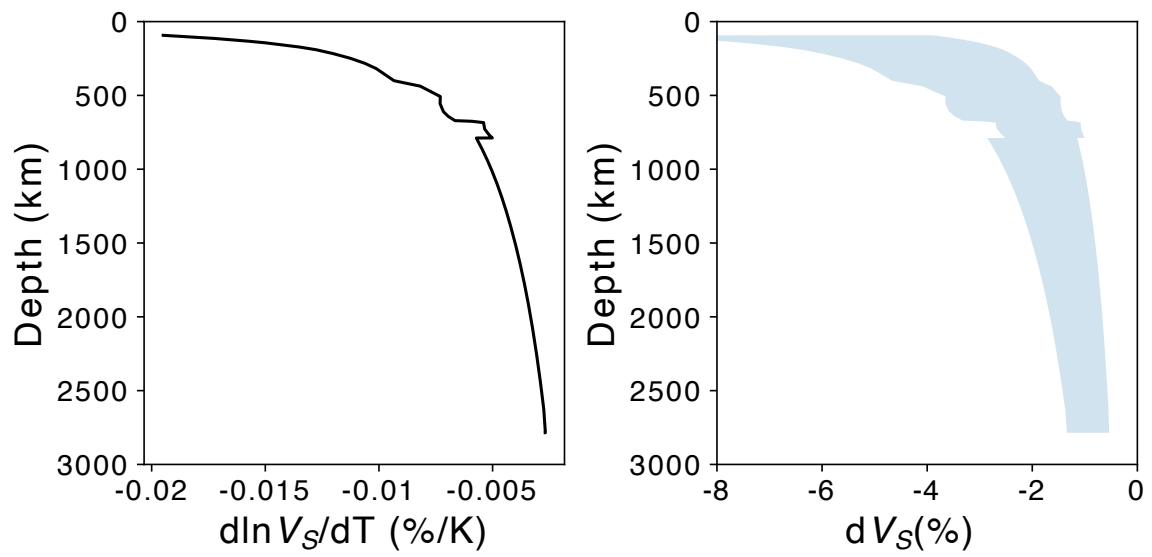
Figure S1. Sensitivity of shear velocity anomaly (left) and the reference δVs (right) with a bulk composition of pyrolite. The reference δVs profile (the blue shaded region) is calculated from the $\delta lnVs/dT$ profile assuming a purely thermal plume with excessive temperatures between 200 and 500 K along depths.
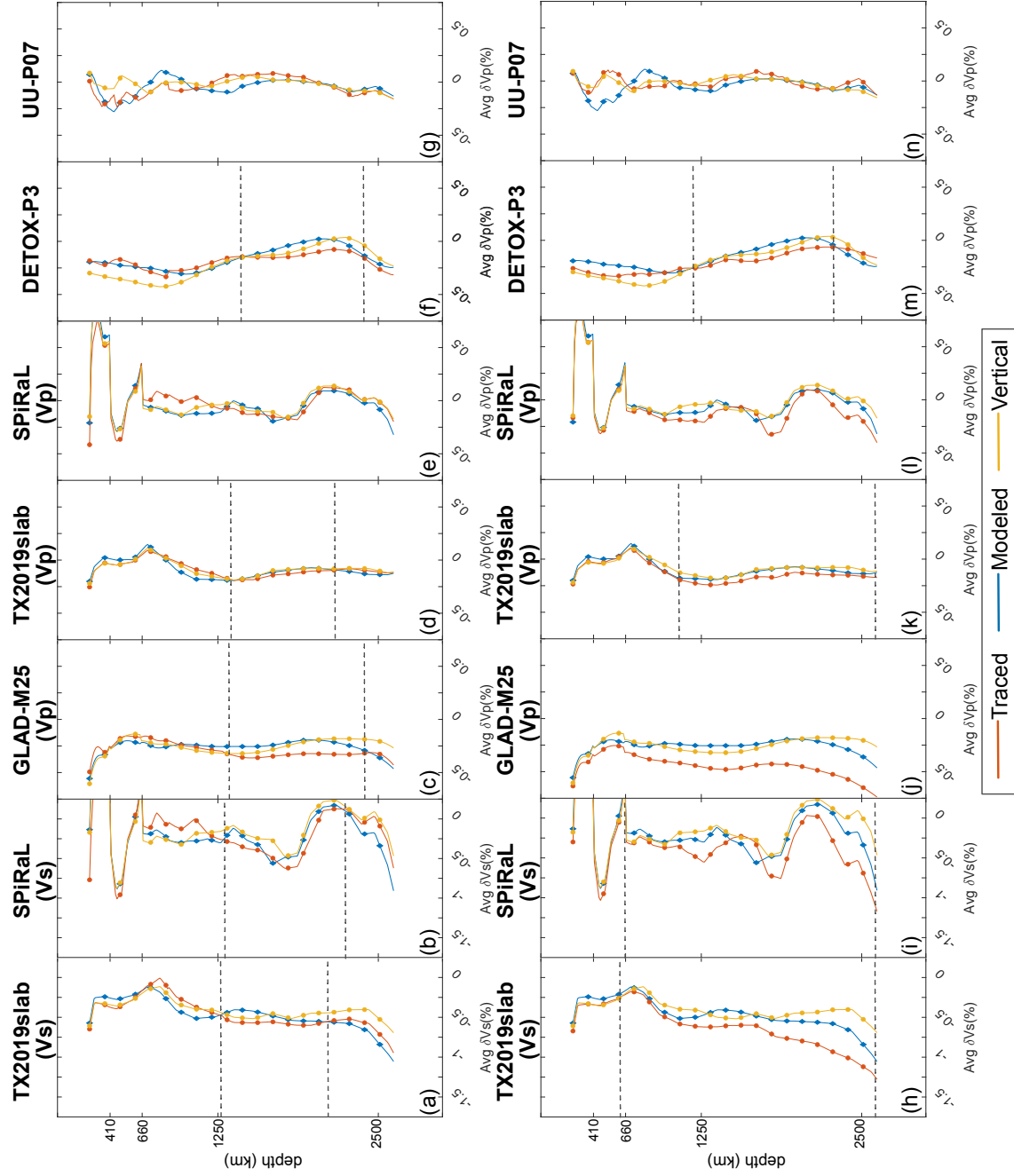
March 30, 2024, 11:35pm

Figure S2. Average δV_S along 12 Pacific traced, model-predicted, and vertical plume conduits (same as Figure 5) in S-velocity models TX2019slab (V_S) (a, h), SPiRaL (V_S) (b, i), and P-velocity models GLAD-M25 (V_P) (c, j), TX2019slab (V_P) (d, k), SPiRaL (V_P) (e, l), DETOX-P3 (f, m), UU-P07 (g, n). The top row is the result of the set of traced conduits from SEMUCB-WM1; the bottom row is the result of the set of traced conduits from GLAD-M25 (V_S). The dotted lines indicate the depth range where the traced plume conduits outperform either the model-predicted or vertical plume conduits.
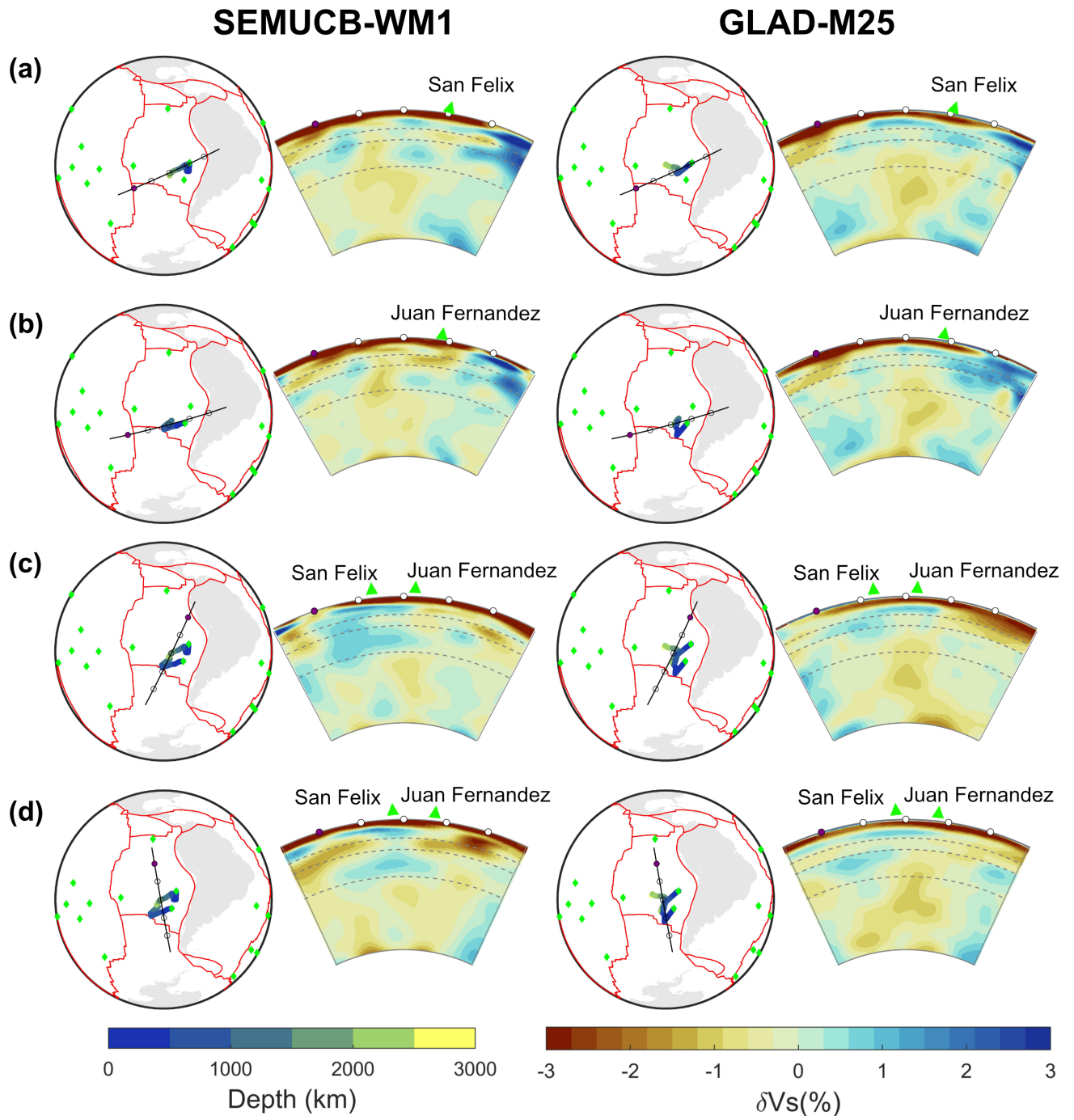
March 30, 2024, 11:35pm

SEMUCB-WM1 **GLAD-M25**

(a)

San Felix

San Felix

(b)

Juan Fernandez

Juan Fernandez

(c)

San Felix Juan Fernandez

San Felix Juan Fernandez

(d)

San Felix Juan Fernandez

San Felix Juan Fernandez

Depth (km)

0 1000 2000 3000

δVs(%)

-3 -2 -1 0 1 2 3

Figure S3. Cross section and map view of the traced conduits of San Felix and Juan Fernandez similar to Figure 8.

March 30, 2024, 11:35pm

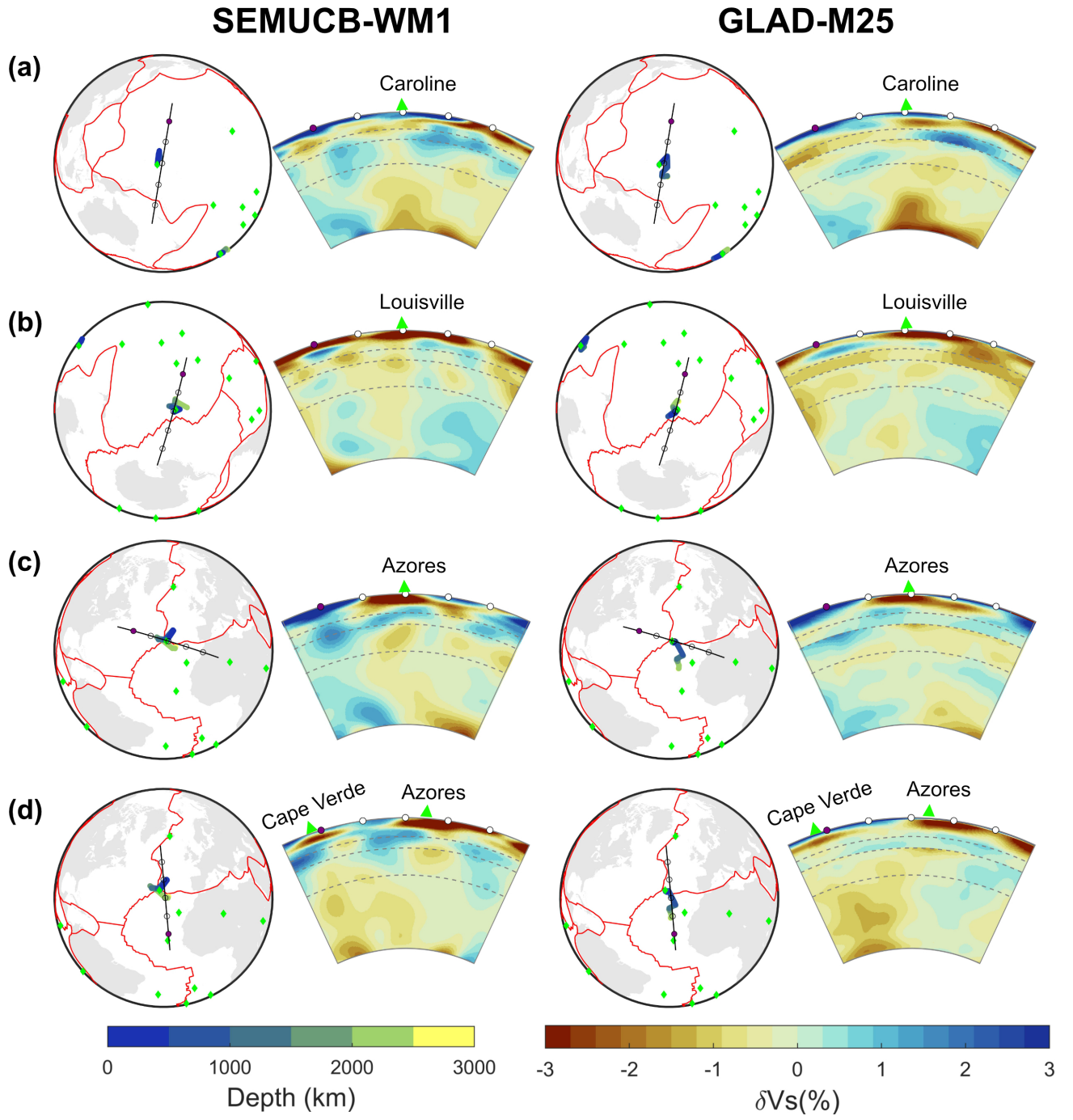**Figure S4.** Cross section and map view of the traced conduits of a) Caroline, b) Louisville, and c,d) Azores similar to Figure 8.

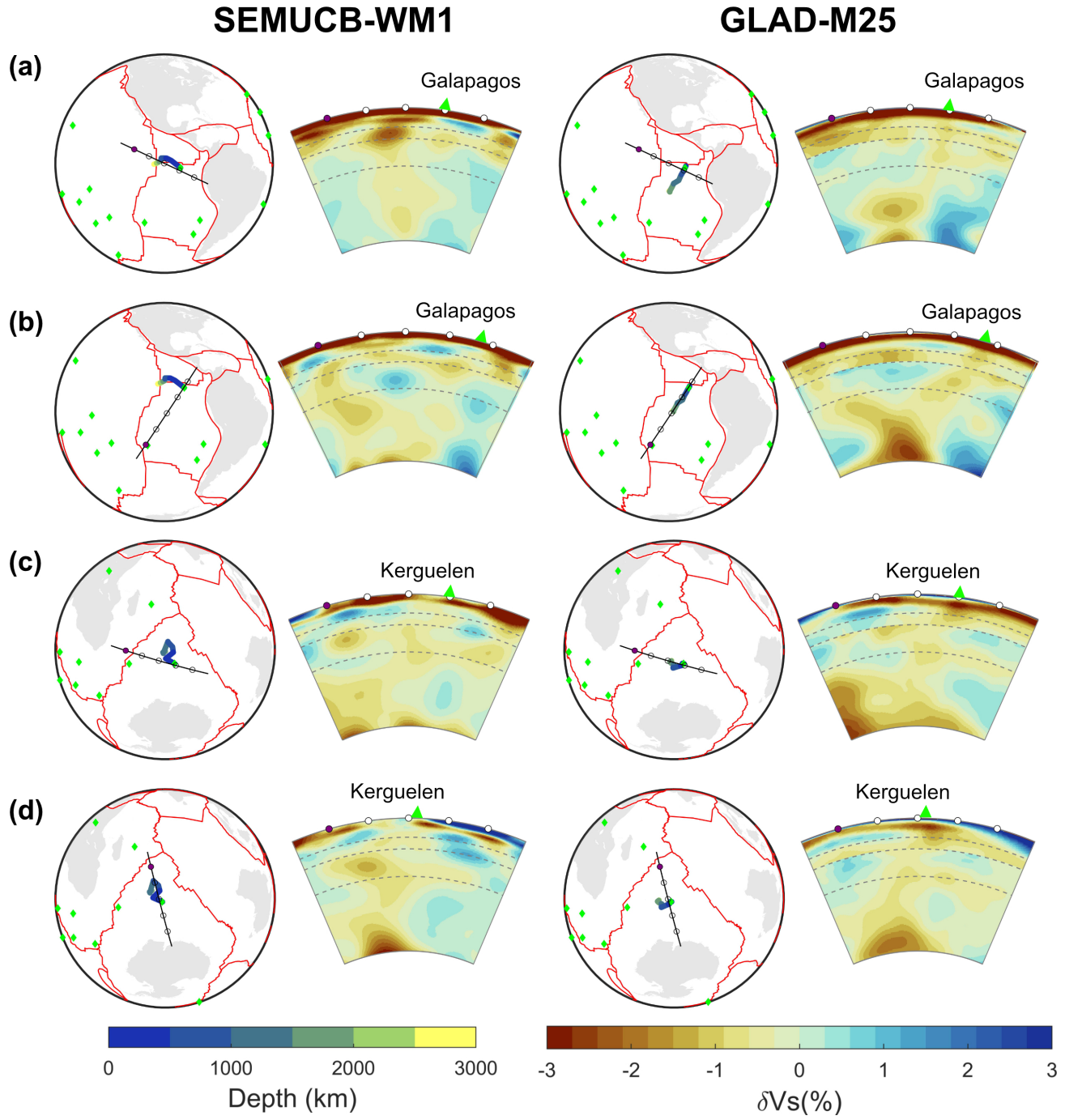**SEMUCB-WM1** **GLAD-M25**

Figure S5. Cross section and map view of the traced conduits of a,b) Galapagos and c,d) Kerguelen similar to Figure 8.
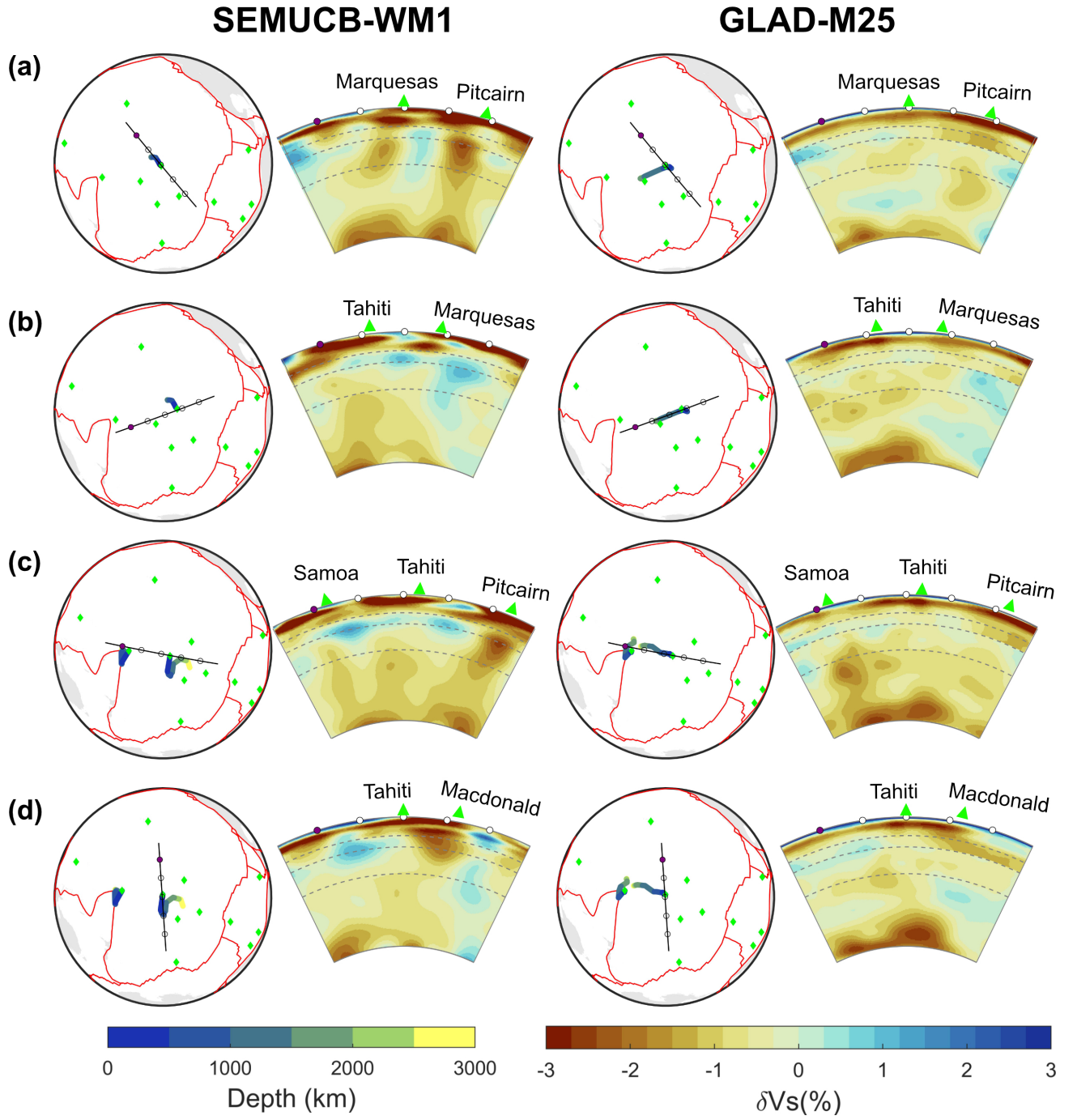
March 30, 2024, 11:35pm

:

Figure S6. Cross section and map view of the traced conduits of a,b) Marquesas and c,d) Tahiti similar to Figure 8.
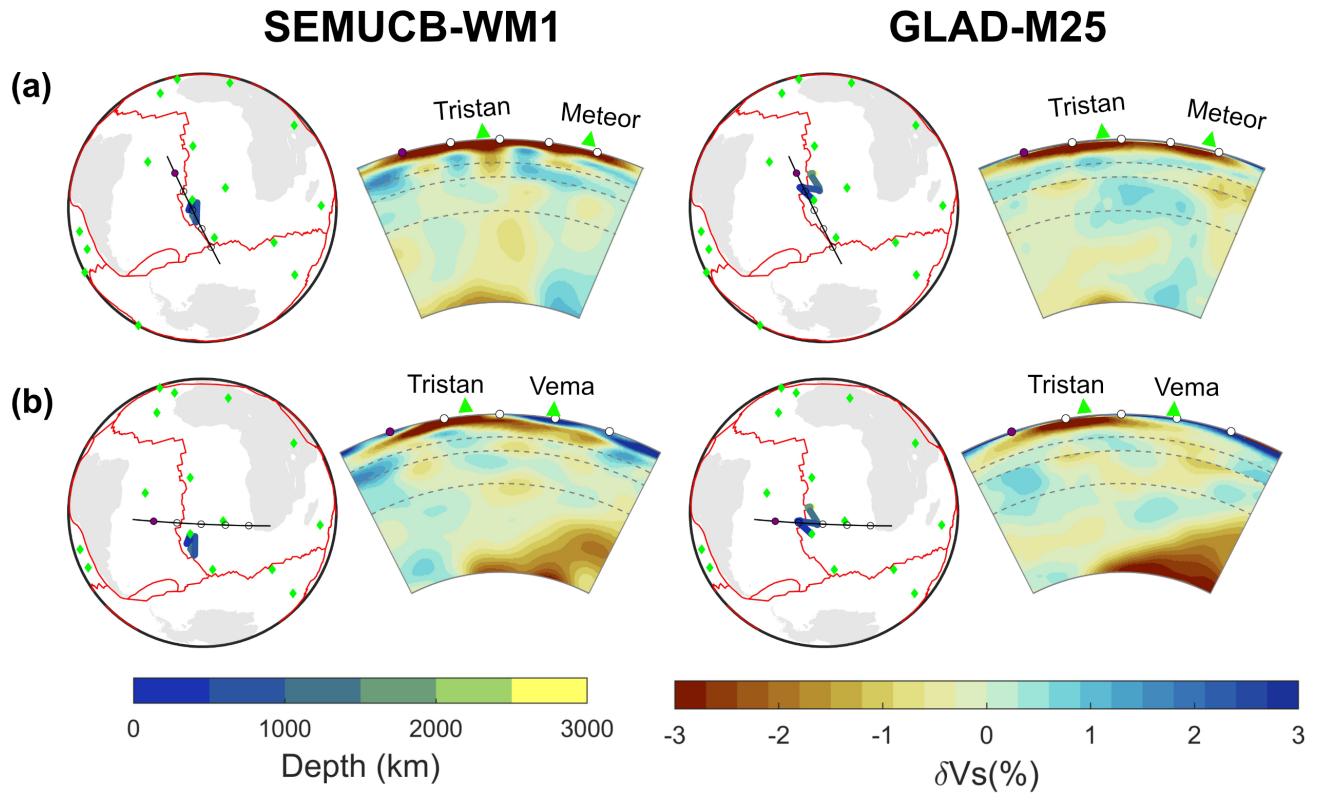
March 30, 2024, 11:35pm

Figure S7. Cross section and map view of the traced conduits of Tristan similar to Figure 8.

:

Table S1. List of plumes traced in this study. The buoyancy flux is obtained from Jackson et al. (2021), the hot spot locations are obtained from Steinberger (2000), and the excess temperature is the petrological estimated excess temperature obtained from Putirka (2008).

Plume	Lat	Lon	Buoyancy Flux $(10^3 kgs^{-1})$	$T_{ex}(K)$	Agree with MC? SEMUCB	GLAD
Azores	38.5°	-28.4°	1.1	124	No	No
Canary	28.0°	-18.0°	0.8	164	Yes	Yes
Cape Verde	15.0°	-24.0°	1.1	114	Maybe	Maybe
Caroline	5.0°	164.0°	1.2	150	No	No
Easter	-27.1°	-109.3°	1.6	N/A	No	No
Galapagos	-0.4°	-91.5°	1.4	130	No	No
Hawaii	19.4°	-155.3°	6.3	290	No	Yes
Iceland	65.0°	-19.0°	5.5	186	Maybe	Maybe
Juan Fernandez	-34.0°	-82.0°	1.7	185	Yes	Yes
Kerguelen	-49.0°	69.0°	1.1	209	Maybe	Yes
Louisville	-51.0°	-138.0°	1.5	200	No	No
Macdonald	-29.0°	-140.2°	3.3	N/A	No	No
Marquesas	-11.0°	-138.0°	3.1	167	Maybe	No
Pitcairn	-25.0°	-129.0°	2.1	189	No	No
Reunion	-21.2°	55.7°	1.4	176	Yes	Yes
Samoa	-15.0°	-168.0°	1.7	223	No	No
San Felix	-26.0°	-80.0°	2.0	N/A	Yes	Yes
St Helena	-17.0°	-10.0°	0.5	164	Yes	Yes
Tahiti	-17.9°	-148.1°	3.7	185	No	No
Tristan	-38.0°	-11.0°	1.0	176	No	No